Fluorescence Resonance Energy Transfer Shows a Close Helix−Helix Distance in the Transmembrane M13 Procoat Protein†

Martin Eisenhawer,‡ Serge Cattarinussi,‡ Andreas Kuhn,§ and Horst Vogel*,‡

Institute of Physical Chemistry, Swiss Federal Institute of Technology, CH-1015 Lausanne, Switzerland, and Institute of Microbiology and Molecular Biology, University of Hohenheim, D-70593 Stuttgart, Germany

Received April 16, 2001; Revised Manuscript Received July 16, 2001

ABSTRACT: During the membrane insertion process the major coat protein of bacteriophage M13 assumes a conformation in which two transmembrane helices corresponding to the leader sequence and the anchor region in the mature part of the protein coming into close contact with each other. Previous studies on the molecular mechanism of membrane insertion of M13 procoat protein have shown that this interaction between the two helices might drive the actual translocation process. We investigated the intramolecular distance between the two helices of the transmembrane procoat protein by measuring fluorescence resonance energy transfer (FRET) between the donor (Tyr) placed in one helix and the acceptor (Trp) placed in the other helix. Various mutant procoat proteins with differently positioned donor−acceptor pairs were generated, purified, and reconstituted into artificial lipid bilayers. The results obtained from the FRET measurements, combined with molecular modeling, show that the transmembrane helices are in close contact on the order of 1−1.5 nm. The present approach might be of general interest for determining the topology and the folding of membrane proteins.

Our present knowledge about the structure and function of membrane proteins originates to a large extent from either molecular biological approaches (*1*−*3*) or investigations of purified components reconstituted under nonphysiological conditions using sophisticated biophysical techniques (see reviews in refs *4*, *5*, and *6*). In this context, diffraction methods (X-ray, electron) and NMR spectroscopy are the most powerful for delivering high-resolution 3D structures of proteins. However, these approaches usually require large quantities of proteins and, in the case of membrane proteins, are still of limited success, because of either difficulties in obtaining suitable crystals for diffraction studies or technical limitations related to protein size as in the case of NMR spectroscopy. For these reasons, alternative methods for monitoring the structure and dynamics of membrane proteins in a membrane environment would be a valuable tool for understanding their interactions in the context of a biologically relevant system.

Here, we use fluorescence resonance energy transfer (FRET)[1] to elucidate the folding of a transmembrane protein, the precursor (=procoat protein) of the coat protein of the filamentous phage M13. The major coat protein of bacteriophage M13 is transiently inserted into the inner membrane of *Escherichia coli* prior to its assembly onto progeny phage particles. The protein is synthesized as a precursor protein of 73 amino acid residues comprising two hydrophobic stretches, one in the 23 amino acid long amino-terminal leader sequence and the other in the mature part near the C-terminus (Figure 1). The process of membrane insertion has been shown to be independent of the preprotein translocase SecYEG and SecA (*7*, *8*). M13 procoat protein readily binds to the membrane surface after leaving the ribosome, and no molecular contact could be detected to the known chaperones and targeting systems (*9*). The membrane insertion is mainly driven by hydrophobic interactions (*10*), but the negatively charged hydrophilic loop is finally translocated with the help of the electrochemical membrane potential and the YidC protein (*11*−*13*).

The procoat protein has been purified, reconstituted into artificial lipid bilayers, and investigated by circular dichroism and infrared spectroscopy (*14*). These measurements have shown that the procoat protein adopts a preferential α-helical conformation in lipid membranes, compatible with a model where the hydrophobic segments of the protein are α-helical. These hydrophobic helices are required for the membrane insertion−translocation of the M13 procoat protein. Mutations in the procoat protein sequence, such as introducing an arginine residue in the hydrophobic stretches of the leader and/or the mature part, have been shown to affect translocation across the membrane. When arginines were placed in both hydrophobic helices, translocation defects were more pronounced than for the single amino acid mutations. Similarly, when the conformation of the α-helix of both hydrophobic regions was affected, e.g., by mutations intro-

† This work was supported by the Swiss National Science Foundation and Interdepartmental Grants of the EPFL to H.V. and by the DFG Sonderforschungsbereich SFB 495 to A.K.

* To whom correspondence should be addressed at EPFL-LCPPM, CH-1015 Lausanne, Switzerland. Tel: +41.21.693.3155. Fax: +41.21.693.6190. E-mail: horst.vogel@epfl.ch.

‡ Swiss Federal Institute of Technology.

§ University of Hohenheim.

[1] Abbreviations: FRET, fluorescence resonance energy transfer; MD, molecular dynamics; POPC, 1-palmitoyl-2-oleoyl-*sn*-glycero-3-phosphocholine; POPE, l-palmitoyl-2-oleoyl-*sn*-glycero-3-phosphoethanolamine; POPG, 1-palmitoyl-2-oleoyl-*sn*-glycero-3-phosphoglycerol; DPPC, 1,2-dipalmitoyl-*sn*-glycero-3-phosphocholine; HPLC, high-performance liquid chromatography; TFA, trifluoroacetic acid.

10.1021/bi0107694 CCC: $20.00
Published on Web 09/21/2001

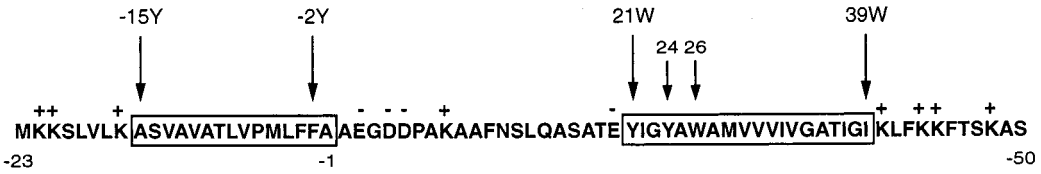

FIGURE 1: Amino acid sequence of H5 procoat protein. The leader sequence comprises amino acid residues −23 to −1 and the mature part +1 to +50. The boxes mark the hydrophobic, putative membrane-spanning segments. Arrows indicate positions of mutations for FRET experiments. The following mutant combinations were constructed (one letter amino acid code is followed by position number): Y−15W21, Y−15W39, and Y−2W21. These mutant proteins comprise always an F at positions 24 and 26. Another mutant protein is W21Y24, which carries an F at position 26.

ducing proline residues, translocation across the membrane was inhibited (*15*). These investigations demonstrated that both hydrophobic helices synergistically contribute to the insertion−translocation event.

We report that the two transmembrane helices are in close proximity to each other, suggesting that a specific interaction between the two protein regions drives the translocation process. This was achieved by constructing, purifying, and membrane-reconstituting mutant procoat proteins containing single intrinsic tyrosine−tryptophan pairs. The Tyr−Trp pair of a particular mutant protein acted as a donor−acceptor couple to measure an intramolecular distance in the procoat protein by FRET. The intramolecular distances obtained by FRET measurements were used as constraints to establish a realistic structural model for the procoat protein spanning a lipid bilayer with two helices. This model served as a basis for additional molecular dynamics (MD) calculations to obtain a realistic picture of the conformational fluctuations of the procoat protein in a lipid bilayer.

FRET is a well-established technique (*16*) to measure intra- and intermolecular distances in water-soluble and membrane proteins (*17*−*19*). Recently, site-specific introduction of nonnatural fluorescent groups into the protein was used to measure FRET even in unpurified, native membranes (*20*, *21*). However, there is a potential risk of modifying the function of the native protein by these methods, and the procedures often are time-consuming. In the present studies, we have used Tyr−Trp as a FRET pair because of the following: (i) These natural amino acid side chains are expected to have no or only minor influence on the protein structure, (ii) additional labeling steps are omitted, and, most importantly, (iii) the short FRET efficiency range [Förster distance $R_0 = 1-1.5$ nm (*22*)] makes it possible to obtain short distance structural constraints. The present approach might be of general interest for determining membrane protein insertion and folding.

MATERIALS AND METHODS

Chemicals. The lipids 1-palmitoyl-2-oleoyl-*sn*-glycero-3-phosphocholine (POPC), l-palmitoyl-2-oleoyl-*sn*-glycero-3-phosphoethanolamine (POPE), and 1-palmitoyl-2-oleoyl-*sn*-glycero-3-phosphoglycerol (POPG) were from Avanti Polar Lipids (Birmingham, AL); all other chemicals were from Fluka (Buchs, Switzerland) and of the best quality available.

Purification of Proteins and Preparation of Proteoliposomes. Procoat mutant proteins were constructed by oligonucleotide-directed mutagenesis (*8*), expressed in *E. coli* LC137 (*14*), and purified by HPLC as described elsewhere for the H5 procoat protein (*14*). Final concentrations of protein were approximately 0.5 mM in acetonitrile/2-propanol/0.02% TFA, determined by the optical density at 280 nm using $\epsilon = 8000\ M^{-1}\ cm^{-1}$ (*14*). The buffer used in the experiments was 1 mM Tris-HCl/0.1 mM EDTA, pH 7.4, degassed with He. Proteins were reconstituted into lipid bilayers at a molar lipid-to-protein ratio of 500 by mixing organic solutions of the procoat protein and lipids, evaporating the solvent, and rehydrating the mixed lipid/protein film in buffer followed by 1 min ultrasonication. This method results in a transmembrane conformation of the reconstituted proteins, as has been shown elsewhere (*10*). Lipid mixtures of POPC/POPG = 4/1 (mol/mol) and POPE/POPC/POPG = 3/1/1 were used for vesicle formation.

Characterization of the Size of Proteoliposomes. Quasielastic light scattering experiments have been performed to characterize proteoliposomes of different composition as described before. A He−Ne laser (632 nm) was used as a light source. The sample was placed in a variable angle goniometer. Light scattering data obtained at different angles were analyzed with a Brookhaven BI-2030 AT digital correlator. Data were evaluated acoording to standard procedures (*23*). Proteoliposomes comprising POPC/POPG = 4/1 showed an average diameter of 55 nm (±12 nm at half-height of distribution histogramme); those of POPE/POPC/POPG = 3/1/1 had an average diameter of 44 nm (±10 nm).

Fluorescence Measurements. Fluorescence measurements were performed using a Spex Fluorolog fluorometer as described in detail elsewhere (*10*). All studies were conducted at room temperature using $1 \times 1\ cm^2$ quartz cuvettes (Hellma, Germany). To reduce light scattering in the presence of liposomes, the fluorescence was measured with crossed polarizers (excitation polarizer horizontal, emission polarizer vertical). Slits were adjusted to 5 nm bandwidths both for excitation and for emission. Excitation spectra were taken from 250 to 330 nm in 1 nm steps at a fixed emission wavelength of 340 nm. Emission spectra were taken from 300 to 450 nm in 1 nm steps at fixed excitation wavelengths of either 280 or 295 nm. The sampling time was 5 s at each wavelength. The spectra were excitation-corrected by referencing to a Rhodamine quantum counter and corrected by subtraction of blank solutions containing lipid vesicles without protein in buffer. Under these conditions, the fluorescence intensity increases linearly with concentration of procoat protein.

Tyrosine emission spectra were obtained by subtracting the spectra recorded by excitation at 295 nm from the spectra recorded by excitation at 280 nm, after normalization of the two emission spectra to identical intensity at 380 nm where Tyr fluorescence is negligible and only Trp fluorescence contributes.

Molecular dynamics simulations were used to create a full atom model of the procoat protein in a hydrated lipid bilayer. As a starting point, we used a water−lipid system consisting of 72 DPPC and 3816 water molecules. The atom coordinates of the lipid bilayer originate from a previous 30 ns MD simulation performed with the software package GROMACS (*24*) using the GROMOS force field (*25*) with slightly modified lipid parameters (*26*). The obtained atom density distributions as well as lipid order parameters are in very good agreement with the corresponding, experimentally determined bilayer properties.

The atom coordinates of M13 procoat protein were first generated as a perfect α-helix using Insight II, a molecular editor from Molecular Simulations Inc. Then, a turn between amino acid Ala10 and Ser13 was created by rotating the three backbone dihedral angles $\phi 11$, $\psi 11$, and $\psi 12$ which delivered the best agreement with the distance constraints derived from our fluorescence experiments.

The process of insertion of a polypeptide into a lipid bilayer takes too long a time to be fully described by a MD simulation. It is therefore necessary to incorporate the polypeptide into the bilayer in a different way. In an often used procedure, individual lipid molecules are placed stepwise around a polypeptide to reach finally a densely packed membrane (*27*). Subsequently, the bilayer is hydrated by adding a water layer on each side of the membrane. A long MD equilibration phase is then required to allow redistribution of potential and kinetic energies at a particular temperature. Unfortunately, the important parameters for judging the reliability of the simulation, such as lipid order parameters and atom density distributions, are not known in the presence of transmembrane polypeptides. Therefore, this method does not allow to correctly control the simulated evolution of the lipid bilayer. In addition, due to the reciprocal influence of lipids and peptides on their structure, one can expect a slow convergence toward the stationary state of the system.

Therefore, we used in the present case a forced dynamic insertion of the M13 procoat protein into a preformed lipid bilayer. This method reduces the above-mentioned problems considerably. We started the process by placing the folded M13 procoat protein with its helices perpendicular to the surface of a hydrated membrane. The atomic coordinates were taken from a correctly preformed, equilibrated lipid bilayer.

The dimension of the simulation box was extended in order to include the protein. Periodic boundary conditions in the $x-y$ membrane plane offered the lipids at the periphery a homogeneous environment. On the contrary, due to the presence of the M13 procoat protein on one side of the lipid bilayer, a water−vacuum interface was created applying periodic boundary conditions in the z-direction. To avoid an influence of this vacuum−water interface on the hydrated lipid bilayer structure (e.g., change of solvent density by diffusion of solvent molecules into vacuum space), the following constraints were imposed on the vertical positions $Z^{\{k\}}$ of the ensemble of all atoms $\{k\}$, by adding the following harmonic term to the MD force field

$$H(Z^{\{k\}}) = \sum_{\{k\}} A(Z^{\{k\}} - Z_0{}^{\{k\}})^2 \qquad (1)$$

where the ensemble of all atoms is defined as $\{k\} = \{$solvent atoms + lipid atoms$\}$ and $Z_0{}^{\{k\}}$ represents the positions of atoms $\{k\}$ in the initial configuration, A being the strength of constraints. The solvent and lipid molecules are free to move in the $x-y$ plane. For the M13 procoat protein similar harmonic constraints were used in the $x-y$ membrane plane, while for the z-direction we shifted $Z_0{}^{\{k\}}$ by a value D toward the membrane obtaining $Z_1{}^{\{k\}} = Z_0{}^{\{k\}} + \Delta$. Subsequently, we started a 10 ps MD run at the end of which − due to constraints − the z coordinates of the polypeptide were such that $Z^{\{k\}} \approx Z_1{}^{\{k\}}$. We then shifted $Z_1{}^{\{k\}}$ to $Z_2{}^{\{k\}} = Z^{\{k\}} + \Delta$. This procedure was repeated several times until the hydrophobic helix parts were centered in the lipid bilayer.

The M13 procoat protein reached the required position after 27 iterations of the described process. During insertion the system was weakly coupled to a temperature and pressure reservoir. The reference temperature and time constant for temperature coupling were set to 320 K and 0.1 ps while the reference pressure and the time constant for pressure coupling were set to 1 bar and 2 ps, respectively. The compressibility in the membrane plane was chosen to be 4.5×10^{-5} (1/bar), while in the z-direction it was set to zero, preventing the simulation box from shrinking perpendicularly to the membrane. The other critical MD control parameters, for instance, the cutoffs of electrostatic and van der Waals interactions, were chosen according to successful lipid bilayer simulations performed with the same force field.

At the end of the insertion process the overall configuration of the lipid and solvent molecules was well conserved. Nevertheless, an excess amount of potential energy had been injected into the system. To prevent perturbations, we chose to release the harmonic constraints in eq 1 while running the system at very low temperature (20 K) for approximatively 1 ns. Another 1 ns run at a temperature of 320 K was performed in order to obtain a well-equilibrated system with stable kinetic and potential energy distribution. This insertion−equilibration stage was followed by a 7 ns MD run.

RESULTS

Donor−Acceptor Pairs in the M13 Procoat Protein. Site-directed mutagenesis was used to introduce tryptophan and tyrosine residues at the desired positions. In a first step, all Tyr and Trp codons of the noncleavable H5 procoat mutant (*28*) were modified into codons for Phe. In particular, the two Tyr residues at positions 21 and 24 and the Trp at position 26 were substituted. The H5 mutant protein was used as a template to place donor−acceptor pairs at desired positions (Figure 1). To investigate the distance between the putative helical leader sequence and the mature coat protein part, we created different mutant proteins comprising one Tyr donor in the first and one Trp acceptor in the corresponding second segment. In particular, Tyr was placed at either position −15 or −2 and Trp at either position 21 or 39. Thus, the engineered donor−acceptor pairs were always located at the corresponding ends of the predicted helical segments as shown in the model in Figure 2. Furthermore, a mutant protein comprising Trp at position 21 and Tyr at position 24 was constructed. Due to the folding-independent short distance between these two amino acid residues, this protein was taken as a reference for 100% energy transfer.

Biological Activity of the Constructed Procoat Mutant Proteins. All mutants were tested in a pulse−chase experi-

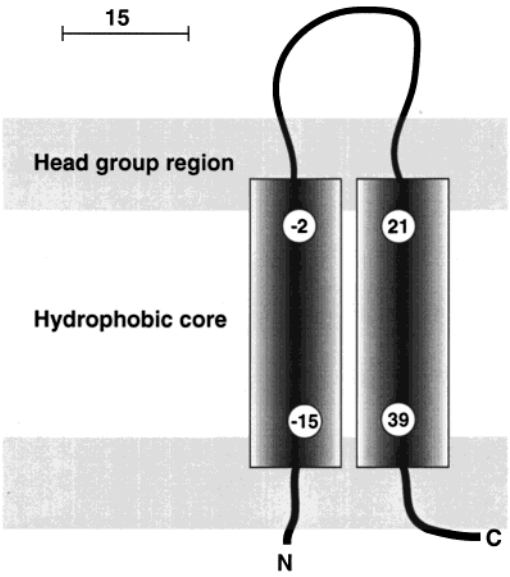

FIGURE 2: Model of the transmembrane conformation of M13 procoat protein comprising two adjacent transmembrane helices. The positions of mutations in the leader sequence (Tyr) and in the mature coat protein (Trp) are indicated.

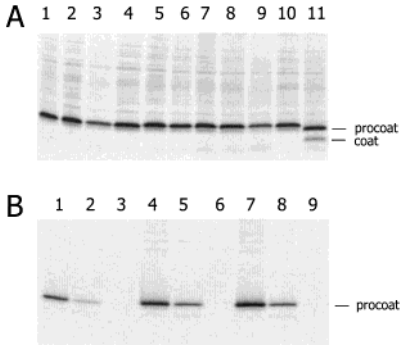

FIGURE 3: Synthesis and membrane integration of M13 procoat protein mutants. (A) *E. coli* LC 137 cells bearing the respective plasmid were grown at 30 °C, pulse-labeled for 3 min (odd-numbered lanes), and subsequently chased with nonradioactive methionine for 3 min (even-numbered lanes). The cells were acid precipitated and resuspended in 2% SDS/20 mM Tris-HCl, pH 8. The proteins were immunoprecipitated with antibodies to M13 phage and analyzed by SDS−PAGE. The mutants F21F24F26 (lanes 1 and 2), W21Y24 (lanes 3 and 4), Y−15W39 (lanes 5 and 6), Y−15W21 (lanes 7 and 8), and Y−2W21 (lanes 9 and 10) were analyzed. As a control, cells expressing wild-type M13 procoat and coat protein were pulse labeled for 30 s (lane 11). (B) Proteinase mapping of M13 procoat mutants. Exponentially growing *E. coli* LC 137 with the respective plasmid were pulse-labeled for 3 min and converted to spheroplasts (lanes 1, 4, and 7). Proteinase K (1 mg/mL) was added and kept on ice for 60 min in the absence (lanes 2, 5, and 8) or presence of Triton X-100 (lanes 3, 6, and 9). The spheroplasts were acid-precipitated, immunoprecipitated, and analyzed by SDS−PAGE. The mutant proteins W21Y24 (lanes 1−3), Y−15W39 (lanes 4−6), and Y−15W21 (lanes 7−9) are shown.

ment to determine if they remained uncleaved and integrated in the cytoplasmic membrane. Exponentially growing *E. coli* LC137 cells bearing the respective plasmids were pulse-labeled with [^{35}S]methionine for 3 min and chased with nonradioactive methionine for an additional 3 min. The analysis of the procoat protein by immunoprecipitation and PAGE revealed that the processing of the mutants was inhibited and the protein remained stable during the chase period (Figure 3A). Due to the mutation at position −3 (Ser → Phe), all procoat mutant proteins are slightly retarded in

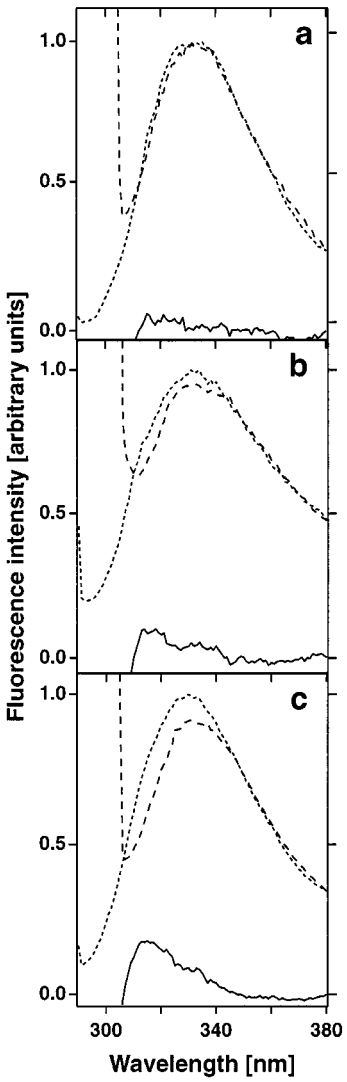

FIGURE 4: Fluorescence emission spectra of procoat mutant proteins incorporated into lipid vesicles of POPC/POPG = 4/1 (molar ratio): short dashed lines, excitation at 280 nm; long dashed lines, excitation at 295 nm; continuous lines, difference spectra ($I_{280} - I_{295}$). Panels: (a) procoat mutant protein W21Y24; (b) Y−15W39; (c) Y−15W21.

their electrophoretic mobility. Membrane translocation of the mutant proteins was tested by the protease mapping technique (Figure 3B). The *E. coli* cells that had been pulse-labeled and chased for 3 min were cooled to 0 °C and treated with lysozyme in the presence of EDTA to form spheroplasts. Proteinase K was added to the outside of the spheroplasts to digest the translocated proteins. The M13 procoat proteins were immunoprecipitated before and after proteolysis. We found that the majority of the Y21W24, Y−15W21, and Y−15W39 mutant proteins were digested, indicating that all of the procoat proteins were normally translocated into the *E. coli* membrane.

Experimental Fluorescence Data. In the following, we use both emission and excitation spectra to obtain information about donor−acceptor distances.

Fluorescence Emission Spectra. Figure 4 shows emission spectra (excitation at 280 and 295 nm) of the different mutant procoat proteins reconstituted in vesicles of POPC/POPG = 4/1 (molar ratio). Fluorescence spectra of the proteins reconstituted in lipid vesicles of POPE/POPC/POPG = 3/1/1,

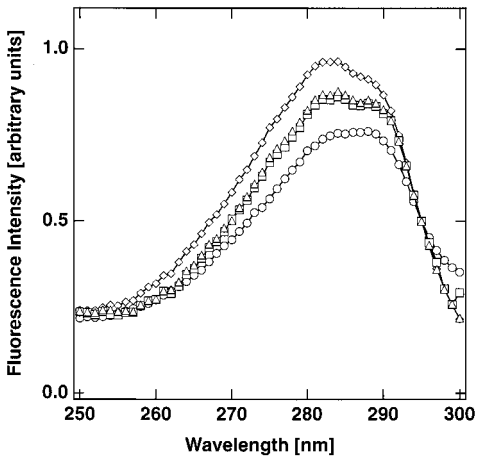

FIGURE 5: Fluorescence excitation spectra (emission detected at 340 nm) of procoat mutant proteins in vesicles of POPC/POPG = 4/1: (◇) W21Y24, (△) Y−2W21, (□) Y−15W39, and (○) Y−15W21.

a composition which is similar to that of the native *E. coli* inner membrane, showed the same characteristics as before, notably the same positions of the emission maxima (data not shown). Therefore, we believe that the following results are representative for the native case of protein insertion.

At 280 nm, both Tyr and Trp are excited. At this excitation wavelength, energy transfer may or may not occur depending upon a number of factors such as the intramolecular distance between the donor and the acceptor FRET pair. Excitation at 295 nm exclusively excites the acceptor Trp, and the distance to the Tyr residue does not influence the emission spectra, unless it has direct contact with the tryptophan's indole ring, which might lead to fluorescence quenching. From the difference spectra ($I_{280} - I_{295}$) in Figure 4 the following cases can be distinguished.

Case 1: No Energy Transfer between Tyr and Trp. The difference spectrum should correspond to the Tyr emission spectrum of the procoat protein since the spectrum obtained from excitation at 280 nm is a sum of fluorescence intensities arising from both Tyr and Trp, whereas the spectrum obtained from excitation at 295 nm is a pure Trp emission spectrum.

Case 2: Total Energy Transfer between Tyr and Trp. The difference spectrum should be zero for all wavelengths, since, independent of the excitation wavelength, pure Trp emission spectra are subtracted and differences in effective quantum yield have been leveled out by normalization of the intensities at 380 nm.

Case 3: Energy Transfer Efficiencies between 0% and 100%. The difference spectra should show a Tyr emission spectrum with intensities varying between 100% and 0%.

The resulting difference spectra depicted in Figure 4 demonstrate the following: (1) Efficient FRET occurs in the mutant procoat W21Y24 protein. (2) Practically no energy transfer is observed in the mutant protein Y−15W21. (3) For Y−15W39 the situation is between the two extreme cases mentioned before.

Fluorescence Excitation Spectra. Figure 5 shows excitation spectra of the different procoat mutant proteins. The spectra were recorded at an emission wavelength of 340 nm, where fluorescence originates exclusively from Trp. The excitation spectra are normalized to equal intensity when excited at 295 nm, where only Trp is excited and thus energy transfer cannot occur. Again, the situations for the two extreme cases are considered.

Case 1: No Energy Transfer between Tyr and Trp. The excitation spectrum is a pure Trp spectrum with the intensities corresponding to the quantum yields at the particular wavelengths.

Case 2: Total Energy Transfer between Tyr and Trp. The excitation spectra show higher intensities at wavelengths below 295 nm where Tyr and Trp are excited simultaneously. FRET from Tyr to Trp increases the measured Trp fluorescence intensity at 340 nm.

Evaluation of Fluorescence Data. A method of analysis originally developed by Eisinger (*22*) is used here and is briefly described. The excitation spectra (emission observed at 340 nm) for various mutant proteins are compared with theoretical spectra for $E = 100\%$, 50%, and 0% transfer efficiency between Tyr and Trp. For this purpose, all excitation spectra are first normalized to identical emission intensity when excited at 295 nm. At this excitation wavelength fluorescence arises exclusively from Trp. Supposing that Trp residues of all different mutant proteins are in a similar environment (as is justified by the practically identical fluorescence spectra of these proteins, shown above), the spectra are normalized to identical intensity at 295 nm, i.e., to identical Trp fluorescence quantum yield. At wavelengths lower than 295 nm, Trp and Tyr are excited simultaneously, and the observed fluorescence signal is a function of the quantum yields of both Trp and Tyr. Because the emission in these experiments was recorded at 340 nm, where only Trp emission occurs, the contribution of Tyr is only visible if energy transfer from Tyr to Trp takes place. A 100% energy transfer yields the highest possible fluorescence intensity for the excitation spectra observed here.

W21Y24 was used to obtain the reference spectrum for 100% energy transfer between its single Tyr and its single Trp, as shown by the fluorescence emission spectra reported in Figure 4. Subtraction of the excitation spectrum of W21Y24 from the excitation spectrum of the particular mutant protein of interest yields the "excitation difference spectra" shown in Figure 6. It is obvious that a mutant protein showing complete energy transfer (as for the case of W21Y24) yields a flat line of relative fluorescence intensity of 1 at all wavelengths. Spectra of the mutant proteins showing less efficient energy transfer than W21Y24 give rise to relative fluorescence values less than 1 in the spectral region where Tyr absorbs (260−295 nm). The theoretical curves for 50% and 0% transfer efficiency shown are calculated from the quantum yields of both Tyr and Trp (see also Figure 4). Mutants Y−15W39 and Y−2W21 both showed an energy transfer of about 50%, whereas the transfer of the mutant Y−15W21 corresponds to a value of $E = 0\%$. We conclude from these data that the residues at positions −15 and 39, and at −2 and 21, are at a distance close to $R_0 = 1-1.5$ nm, whereas the residues at −15 and 21 are at a distance considerably larger than R_0.

Molecular Dynamics Simulation. The intramolecular distance constraints obtained by FRET measurements were the basis for constructing the structure of M13 procoat protein in the MD simulation. A U-shaped protein, comprising two adjacent, ideal straight α-helices, was gradually inserted into the lipid bilayer during a MD simulation run. The desired

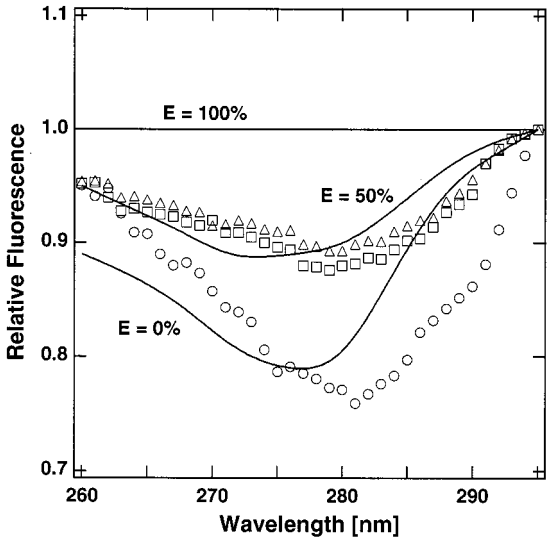

FIGURE 6: Fluorescence excitation spectra (emission at 340 nm) of the mutant proteins (△) Y−2W21, (□) Y−15W39, and (○) Y−15W21 are compared with theoretical curves from ref *22* calculated for different efficiencies for the Tyr−Trp energy transfer.

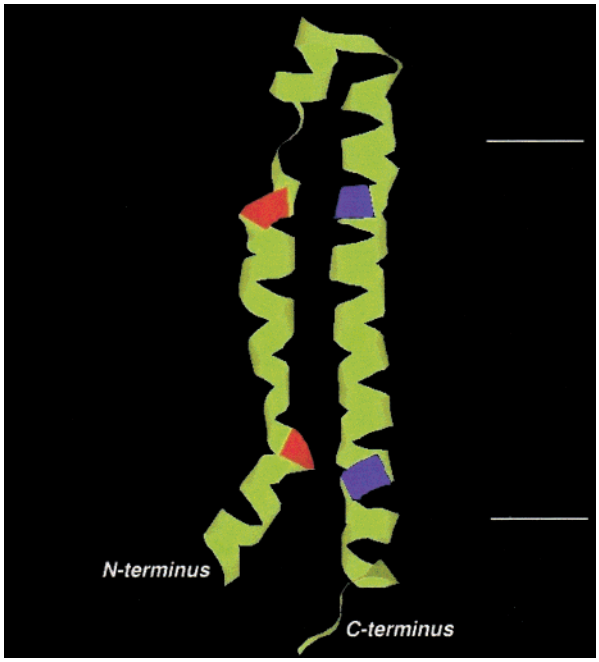

FIGURE 7: Structure of the procoat protein in a hydrated, fluid DPPC lipid bilayer obtained from a MD simulation. The procoat protein is first folded to form a hairpin comprising two straight, ideal α-helices. FRET distances between Y−2 and W21, Y−15 and W21, and Y−15 and W39 as well as the helix content measured by circular dichroism are used as constraints. This model served as a starting structure for the MD simulations. Shown is a snapshot of a procoat protein structure after 3 ns of MD simulation. The locations of Tyr residues in the polypeptide backbone are shown in red, and those of the Trp residues are in blue. The hydrophobic part of the lipid bilayer is depicted by two white horizontal lines.

insertion was obtained by applying an external force on each protein atom. Position constraints have been set on the lipid and water molecules during insertion of the protein into the lipid bilayer, preventing them from moving in the direction perpendicular to the membrane plane but still allowing displacements in the membrane plane in order to provide sufficient space for the protein molecule. Within the final MD simulation, the two bilayer-spanning helices performed fluctuations. The hydrophobic part of the mature coat protein sequence deviated only slightly from the starting ideal straight helix conformation; the helix of the leader sequence part, in comparison, showed much stronger conformational deviations from its ideal starting state, especially at the ends of the transmembrane helix (Figure 7). Despite this substantial conformational flexibility, the distances between the particular Tyr−Trp donor−acceptor positions remained quite constant over the entire investigated time regime as shown in Figure 8. We have extended the simulation over a time regime of 9 ns, and the distance fluctuations remain constant within a range of ±0.2 nm (Figure 8). The good agreement between the MD and FRET distances in turn suggests that the MD simulations deliver a reliable description of the real membrane protein structural dynamics.

DISCUSSION

FRET experiments have been shown to be suitable for elucidating the transmembrane conformation of M13 procoat protein. As determined by our quasielastic light scattering experiments, proteoliposomes of a defined size with a narrow size distribution were created by ultrasonication. Taking into account the average size of 55 nm for the POPC/POPG vesicles, each vesicle has a surface area of about 9500 nm^2 corresponding to about 31 000 lipid molecules. Because the molar lipid/protein ratio of the preparation is 500, each vesicle contains then about 60 protein molecules. If specific protein−protein interactions are excluded, an individual procoat protein molecule is surrounded by less than 0.04 protein molecules in a circle of radius = 1.5 nm, the Förster distance R_0 for the Tyr−Trp pair. General methods have been proposed to estimate FRET in a lipid bilayer for systems containing one donor and multiple acceptors (*29*−*31*). Because the value calculated for the intermolecular density of acceptors in the local environment surrounding the donor is negligible, it is clear that FRET in our proteoliposomes is due almost exclusively to the intramolecular energy transfer between the Tyr and the Trp residues of a particular procoat mutant protein.

For obtaining distance information from Tyr−Trp FRET, Eisinger (*22*) proposed two approaches. One approach uses the individual emission spectra of Tyr and of Trp evaluated from the experimental spectrum, which is the sum of the Tyr and Trp emission. In the present work we have used this approach, but unfortunately, our emission spectra showed a substantial amount of light scattering when excited at 295 nm. Thus, the individual Tyr fluorescence spectrum could only be evaluated down to about 315 nm. In principle, it would be possible to fit our data to obtain the maximal fluorescence intensity around 305 nm, but the uncertainty of this approach is rather large. Therefore, we also used the second approach of Eisinger (*22*) to determine the relative quantum yields of Tyr and Trp via their relative absorption of light. The emission spectrum of procoat W21Y24 incorporated into POPC/POPG vesicles shows that the efficiency of Tyr−Trp energy transfer is 100% (see Figure 4), justifying the use of this mutant protein as a reference. The intensity of the fluorescence at 340 nm as a function of excitation wavelengths (i.e., the excitation spectra) for the mutant proteins Y−15W39, Y−2W21, and Y−15W21 normalized to the W21Y24 excitation spectrum is shown in Figure 6.

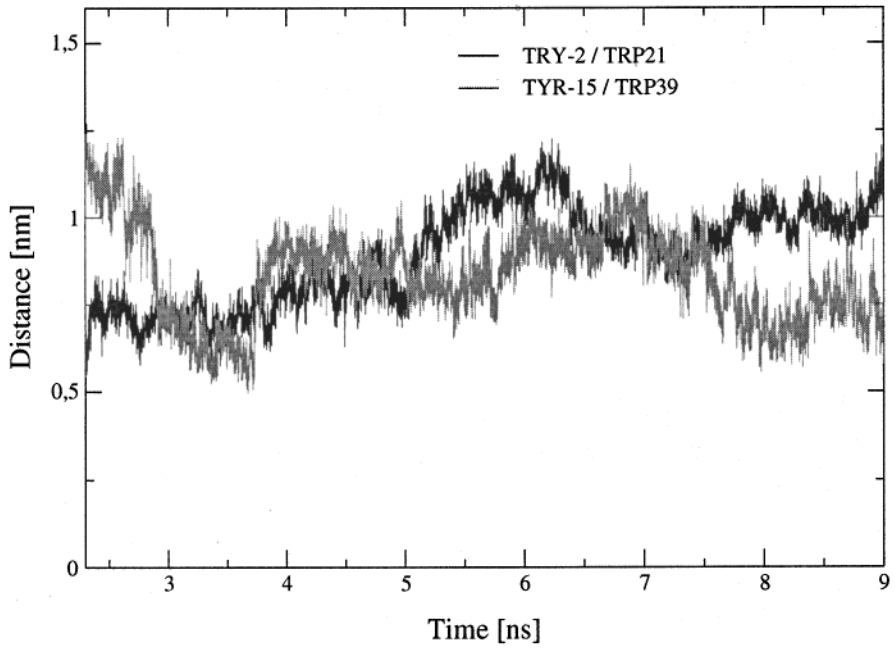

FIGURE 8: Typical time courses of the distances between Tyr and Trp residues in the indicated positions of M13 procoat mutant proteins. Shown are the MD time windows from 2.3 to 9 ns after the different equilibration steps.

For Y−15W39 and for Y−2W21 the experimental data are consistent with half-maximal energy transfer; those for Y−15W21 are consistent with no energy transfer. Taken together, these data give approximate distance values. For example, the distance between Trp39 and Tyr(−15) as well as between Trp21 and Tyr(−2) is on the order of the Förster distance, $R_0 \approx 1$ nm. The distance R between Trp21 and Tyr(−15) is on the order of or larger than $2R_0$, since at distances $R > 2R_0$, no energy transfer will occur (*22*).

A structural model of the membrane-inserted M13 procoat protein is derived from these measurements: The proximity of residues −2 and 21 and residues −15 and 39 obtained from FRET, together with the measured 60% helix content of the transmembrane M13 procoat protein (*14*), provides strong evidence for the hairpin configuration depicted in Figure 2. Although the measured helix content does not allow one to exactly localize α-helices along the amino acid sequence of the protein, it is reasonable to assign helices to the two hydrophobic and putative transmembrane regions in the M13 procoat protein sequence, indicated as rectangles in Figure 2. A more detailed representation is obtained by molecular dynamics calculations shown in Figure 7. It presents a full atom model of the procoat protein inserted in a hydrated DPPC lipid bilayer. Taking into account the helix content of the procoat protein in lipid membranes as measured by circular dichroism and the distance constraints as determined by the FRET experiments in this work, the MD calculations provide a realistic picture of the conformational fluctuations of the procoat protein.

According to these simulations, the procoat protein shows the following features: (1) Only a minor portion of the periplasmic (loop) region faces the free solvent. (2) Most of the N-terminal and of the C-terminal regions are located in the membrane−water interfacial region that shows a reduced access to water as compared to bulk solvent (*32*, *33*). (3) Although the overall hairpin conformation of the procoat protein is stable over the entire time scale of the MD simulations (Figure 8), there is a considerable difference in the mobility of the different parts of the protein. The long hydrophobic helix of the mature coat protein domain remains rather rigid with only small conformational fluctuations at the ends of the helix as had been seen experimentally and in simulations for single, hydrophobic transmembrane helices (*34*, *35*). In contrast, only a rather short segment of the transmembrane helix of the leader sequence remains rigid while both ends of this helix perform substantial conformational fluctuations. As a consequence, the lipid bilayer, facing the membrane-traversing leader sequence portion, is more distorted than the corresponding lipids in contact with the mature coat protein segment (pictures not shown). It will be interesting to investigate the stability of the procoat protein in a future MD simulation over an extended time scale.

Structural studies on the M13 coat protein have suggested a hinge region around residue 23 and an amphipathic helix sitting on the surface of the membrane (*36*, *37*). The conformation of this region in the procoat protein must be clearly different, since an α-helix parallel to the membrane plane would separate the leader sequence and mature transmembrane helices. Possibly, the conformation of this region changes after cleavage by leader peptidase.

The maxima of the Trp fluorescence spectra around 330 nm for all membrane-incorporated procoat mutant proteins indicate a hydrophobic environment of the tryptophan residues located at positions 21, 24, and 39, as well as at positions 26 and 30 (results not shown here). This hydrophobic environment could be either the hydrophobic core of the membrane, the adjacent hydrophobic residues of the leader sequence, or the lipid headgroup region of the membrane. The locations of these residues in Figure 7 are compatible with these restrictions.

Taken together, the fluorescence experiments and the molecular modeling show that the M13 procoat protein is deeply embedded in the membrane with the two transmembrane helices in close proximity to each other. It appears that a major portion of the periplasmic loop is located at the membrane interface and that the site where cleavage by

leader peptidase occurs is at the boundary between the membrane interface and the hydrophobic core. This is consistent with the amphiphilic structure of the leader peptidase, showing that the active center is located between the hydrophobic and hydrophilic parts of the enzyme (*38*).

Several approaches have been employed to investigate interactions between membrane-spanning parts of proteins, e.g., by probing disulfide bond formation between adjacently engineered cysteine residues, by other chemical cross-linking methods, or by interacting spin labels using ESR or NMR (*2*, *3*, *5*, *6*).

In this work, FRET measurements between Tyr and Trp residues have delivered molecular distances of a bilayer-inserted membrane protein. The experimental approach is of general importance for protein structure determination and offers several interesting advantages over presently used methods. It requires no crystals, no structure-perturbing labeling or cross-linking, can be performed with extremely small protein amounts, and if time-resolved measurements are performed, it delivers additional information about distance distributions (*39*, *40*), i.e., about the dynamics of conformational fluctuations of the protein with nanometer space resolution and nanosecond time resolution.

These experimentally obtained distance constraints serve as an important basis for MD simulations which, in turn, can deliver a reasonable dynamical model for the structure of a protein in a lipid bilayer.

ACKNOWLEDGMENT

We thank Robin Humphrey-Baker for performing the quasielastc light scattering experiments, Hanna Jankevics for help in preparing the figures, and the referees for helpful comments. This work benefited from many discussions with Olle Edholm during his sabbatical stay in our Institute.

REFERENCES

1. Haigh, N. G., and Webster, R. E. (1998) *J. Mol. Biol. 279*, 19−29.
2. Armulik, A., Nilsson, I., von Heijne, G., and Johansson, S. (1999) *J. Biol. Chem. 274*, 37030−37034.
3. Monne, M., Nilsson, I., Elofsson, A., and von Heijne, G. (1999) *J. Mol. Biol. 293*, 807−814.
4. White, S. H. (1994) *Membrane Protein Structure*, Oxford University Press, New York.
5. von Heijne, G. (1997) *Membrane Protein Assembly*, Springer, Berlin.
6. Popot, J.-L., and Engelman, D. (2000) *Annu. Rev. Biochem. 60*, 881−922.
7. Wolfe, P. B., Rice, M., and Wickner, W. (1985) *J. Biol. Chem. 260*, 1836−1841.
8. Kuhn, A. (1988) *Eur. J. Biochem. 177*, 267−271.
9. de Gier, J. W., Scotti, P. A., Saaf, A., Valent, Q. A., Kuhn, A., Luirink, J., and von Heijne, G. (1998) *Proc. Natl. Acad. Sci. U.S.A. 95*, 14646−14651.
10. Soekarjo, M., Eisenhawer, M., Kuhn, A., and Vogel, H. (1996) *Biochemistry 35*, 1232−1241.
11. Zimmermann, R., Watts, C., and Wickner, W. (1982) *J. Biol. Chem. 257*, 6529−6536.
12. Cao, G., Kuhn, A., and Dalbey, R. E. (1995) *EMBO J. 14*, 866−875.
13. Samuelson, J. C., Chen, M., Jiang, F., Möller, I., Wiedmann, M., Kuhn, A., Phillips, G. J., and Dalbey, R. E. (2000) *Nature 406*, 637−641.
14. Thiaudière, E., Soekarjo, M., Kuchinka, E., Kuhn, A., and Vogel, H. (1993) *Biochemistry 32*, 12186−12196.
15. Kuhn, A. (1995) *FEMS Microbiol. Rev. 17*, 185−190.
16. Förster, T. (1949) *Z. Naturforsch. 4*, 321−327.
17. Stryer, L. (1978) *Annu. Rev. Biochem. 47*, 819−846.
18. Lakey, J. H., Baty, D., and Pattus, F. (1991) *J. Mol. Biol. 218*, 639−653.
19. Johnson, D. A., and Nuss, J. M. (1994) *Biochemistry 33*, 9070−9077.
20. Turcatti, G., Nemeth, K., Edgerton, M. D., Meseth, U., Talabot, F., Peitsch, M., Knowles, J., Vogel, H., and Chollet, A. (1996) *J. Biol. Chem. 271*, 19991−19998.
21. Cha, A., Snyder, G. E., Selvin, P. R., and Bezanilla, F. (1999) *Nature 402*, 809.
22. Eisinger, J. (1969) *Biochemistry 8*, 3902−3908.
23. Humphry-Baker, R., Thompson, D. H., Lei, Y., Hope, M., and Hurst, J. K. (1991) *Langmuir 7*, 2592−2601.
24. Berendsen, H. J. C., van der Speol, D., and van Drunen. R. (1995) *Comput. Phys. Commun. 91*, 43−56.
25. van Gunsteren, W. F., and Berendsen, H. J. C. (1987) *Library Manual, Biomos, Nijenborgh 4*, 9749.
26. Berger, O., Edholm, O., and Jähnig, F. (1997*) Biophys. J. 72*, 2002−2013.
27. Merz, K. M., Jr., and Roux, B. (1996) *Biological Membranes: A Molecular Perspective from Computation and Experiment*, Birkhäuser, Boston, MA.
28. Kuhn, A., and Wickner, W. (1985) *J. Biol. Chem. 260*, 15914−15918.
29. Dewey, T. G., and Hammes, G. G. (1980) *Biophys. J. 32*, 1023−1035.
30. Estep, T. N., and Thompson, T. E. (1979) *Biophys. J. 26*, 195−207.
31. Wolber, P. K., and Hudson, B. S. (1979) *Biophys. J. 28*, 197−210.
32. White, S. H., and Wimley, W. C. (1998) *Annu. Rev. Biophys. Biomol. Struct. 28*, 319−365.
33. Hristova, K., Wimley, W. C., Mishra, V. K., Anantharamiah, G. M., Segrest, J. P., and White, S. H. (1999) *J. Mol. Biol. 290*, 99−117.
34. Vogel, H., Nilsson, L., Rigler, R., Voges, K.-P., and Jung, G. (1988) *Proc. Natl. Acad. Sci. U.S.A. 85*, 5067−5071.
35. Forrest, L. R., Tieleman, D. P., and Sansom, M. S. P. (1999) *Biophys. J. 76*, 1886−1896.
36. Almeida, F. C. L., and Opella, S. J. (1997) *J. Mol. Biol. 270*, 481−495.
37. Papvoine, C. H., Christiaans, B. E., Folmer, R. H., Konings, R. N., and Hilbers, C. W. (1998) *J. Mol. Biol. 282*, 401−419.
38. Paetzel M., Dalbey R. E., and Strynadka, N. C. J. (1998) *Nature 396*, 186−190.
39. Haas, E., Wilchek, M., Katchalski,-Katzir, E., and Steinberg, I. Z. (1975) *Proc. Natl. Acad. Sci. U.S.A. 72*, 1807−1811.
40. Vogel, H., Nilsson, L., Rigler, R., Meder, S., Boheim, G., Beck, W., Kurth, H.-H., and Jung, G. (1993) *Eur. J. Biochem. 212*, 305−313.

BI0107694